

Effect of Nongray Gas Radiation on Thermal Stability in Carbon Dioxide

J. E. Hutchison*

Fairchild Controls Corporation, Frederick, Maryland 21701-5716
and

R. F. Richards†

Washington State University, Pullman, Washington 99164-2920

The problem of the onset of thermal instability in a horizontal layer of radiatively participating gas, heated from below and cooled from above, is considered. In the present work, both experimental heat transfer measurements across carbon dioxide and air layers before and after the onset of instability and a theoretical analysis of the coupled conduction–radiation heat transfer in the base state of the quiescent carbon dioxide gas layers, just before the onset of instability, are presented. The heat transfer measurements reveal a 7–20% increase in the critical Rayleigh number in the radiatively participating carbon dioxide vs a similar layer of air. Measurements of heat flux before the onset of the instability confirm, within experimental uncertainty, the predictions of the nongray analysis of the coupled conductive–radiation heat transfer problem. The nongray analysis also indicates that the distortion of the initial base-state temperature profiles as a result of gas radiation in the quiescent carbon dioxide gas layers is extremely small. Finally, a 20% reduction in heat transfer, after the onset of the instability, is observed in the carbon dioxide layer, compared with a similar air layer, which persists up to the highest Rayleigh number tested, $Ra = 10^4$.

Nomenclature

A	= band absorptance
A_0	= bandwidth parameter
C_p	= constant pressure specific heat, kJ/kg-K
D	= test cell length, mm
$E_n(x)$	= exponential integral functions
e	= radiosity, W/m ²
g	= gravitational acceleration, m/s
J	= wall radiosities, W/m ²
k	= gas thermal conductivity, W/m-K
L	= gas-layer thickness, mm
N	= $A_0 \tau_0 Le'_b(T_1)/k$
Nu_1	= Nusselt number, defined in Eq. (1)
Nu_2	= Nusselt number, defined in Eq. (2)
P	= gas pressure, kPa
q	= heat flux, W/m ²
Ra	= Rayleigh number, defined in Eq. (3)
T	= temperature, K
W	= test cell width, mm
y	= spatial coordinate
α	= thermal diffusivity, m ² /s
β	= volume coefficient of expansion, K ⁻¹
ΔT	= temperature difference between plates, K
ε	= plate emissivity
θ	= dimensionless temperature, T/T_1
κ	= absorption coefficient, m ⁻¹
λ	= wavelength, m
μ	= dynamic viscosity, N-s/m ²
ν	= kinematic viscosity, m ² /s
ρ	= plate reflectivity
τ	= optical depth

Subscripts

b	= blackbody
cal	= calorimeter
cal, 0	= calorimeter, for quiescent layer, before the onset of instability
m	= mean gas-layer value
R	= radiative
λ	= spectral quantity
1	= lower, hot plate
2	= upper, cold plate

Introduction

INTEREST in the question of the Rayleigh–Benard problem in a radiating fluid was originally motivated by questions about convective heat and mass transfer in stellar and planetary atmospheres. Goody¹ first attacked the problem of convective stability in an atmosphere by putting forward an approximate solution to the problem of the onset of instability in a horizontal layer of radiatively participating gas. Predictions of the critical Rayleigh number, or the Rayleigh number at the onset of instability, were made by extending the linear stability analysis of Pellew and Southwell² to include the contribution of radiative heat transfer from a gray gas.

Gille and Goody³ continued the work with both theoretical and experimental work. In revisiting the problem, they focused on a more realistic treatment of the radiative transfer, which dealt explicitly with the nongray nature of molecular gas radiation by incorporating a statistical narrow-band model for the gas radiation properties. Predictions of the one-dimensional temperature profile in and total heat transfer across the gas layer were made with a coupled conduction–radiation heat transfer analysis. A dimensional argument was used to arrive at an approximate expression for critical Rayleigh number. The predictions of the analysis were tested in a series of experiments in horizontal layers of ammonia gas in which the temperature profiles in and heat transfer across the gas layers were measured using interferometry and heat flux meters. Temperature profiles and total heat transfer rates, measured in the quiescent gas before the onset of the instability, were found to

Received Jan. 15, 1998; revision received June 30, 1998; accepted for publication July 6, 1998. Copyright © 1998 by the American Institute of Aeronautics and Astronautics, Inc. All rights reserved.

*ECS Engineer, 540 Highland Street.

†Assistant Professor, School of Mechanical and Materials Engineering. Member AIAA.

match those predicted by the coupled conduction–radiation analysis, within experimental uncertainty. Critical Rayleigh numbers determined for the radiatively participating ammonia gas layers were found to be significantly larger than those measured in a nonparticipating gas such as air, as predicted by the nongray analysis. However, because of the approximate nature of the instability analysis, the agreement between measured and predicted critical Rayleigh numbers was suggestive, but not conclusive.

Later studies have concentrated either on 1) improving predictions of the onset of instability, or 2) revisiting the analysis of the coupled conduction–radiation heat transfer in the quiescent gas layer before the onset of instability. In the first group, for example, Christophorides and Davis⁴ applied a more rigorous linear stability analysis than Gille and Goody, but accomplished this only by restricting their radiation analysis to a gray gas theory. Arpaci and Gozum⁵ presented a linear stability analysis in which the gas radiation was treated with a semigray analysis. In the semigray analysis the nongrayness of the participating medium was characterized by two parameters formed from the product and the ratio of the Planck and Rosseland mean absorption coefficients. More recently, Neitzel et al.⁶ showed that an energy stability theory could be applied to the Rayleigh–Benard problem in a radiating fluid. However, their analysis was limited to optically thin gray media. In each of these studies, the work was entirely theoretical, with no experimental measurements presented to compare with the analytical predictions.

In the second group, Schimmel et al.⁷ focused on understanding the coupled conduction–radiation heat transfer in the quiescent gas layer in a base state, before the onset of the instability. They first predicted heat transfer across a quiescent gas layer using a coupled conduction–radiation heat transfer analysis and then compared those predictions with heat transfer measurements made in horizontal layers of gas. Measurements were made in four gas mixtures: pure carbon dioxide, pure nitrous oxide, a mixture of carbon dioxide and nitrous oxide, and a mixture of carbon dioxide and methane. The coupled conduction–radiation heat transfer was predicted using three different gas radiation models: a gray gas model, a box or grayband model, and exponential wideband models. The conduction heat transfer across the gas layers was determined by measuring the temperature profiles in the gases using a Mach–Zehnder interferometer. The comparison of measurements with the three sets of predictions showed clear differences between the gray and nongray gas models. While both the gray gas model and the grayband model performed very poorly, the predictions of the wideband exponential model matched the measurements of conductive heat transfer under all conditions tested. Novotny and Olsofka⁸ extended the work of Schimmel et al. by looking at the effect of mixing a nonparticipating gas with an absorbing–emitting gas. Gas mixtures of carbon dioxide and nitrogen and nitrous oxide and oxygen were considered. Once again, agreement between the nongray gas analysis and the measurements was good for all conditions considered.

Numerous other workers have analyzed the coupled conduction–radiation problem in a nongray gas layer. Most notably, Crosbie and Viskanta⁹ solved the problem by assuming a Milne–Eddington-type absorption coefficient to make the treatment of the gas radiation tractable. Soufiani et al.¹⁰ looked at the effect of band models on coupled conduction–radiation heat transfer in a plane gas layer. Gupta et al.,¹¹ and later Smith et al.,¹² considered the effect of the addition of soot to the gas layer. More recently, Kamiuto¹³ applied a two-parameter wideband spectral model for the gas-radiation properties developed earlier.¹⁴ In each of these studies the work was entirely theoretical, with no experimental measurements presented to compare with the analytical predictions.

It is notable that, since Gille and Goody's³ work on the stability problem and Schimmel et al.'s⁷ work on the coupled

conduction–radiation problem, no experimental measurements relevant to the Rayleigh–Benard problem in a radiating fluid have been reported. For this reason the present work was undertaken to experimentally examine the onset of thermal instability in a radiatively participating gas.¹⁵ In the present work, a program of heat transfer measurements across plane layers of both diathermanous and radiatively participating gases is described. Measurements of total heat flux across the gas layers are presented and then used to identify the onset of instability and determine the critical Rayleigh number, Ra_{cr} , for the gas layer. Heat transfer measurements are presented for three different gas layers: air, an air–carbon dioxide mixture, and pure carbon dioxide, at three orientations of the gas layers: 0-deg tilt (horizontal and heated from below), 30-deg tilt from horizontal, and 180-deg (horizontal and heated from above). In addition, an analysis of the coupled conduction–radiation problem in a nongray gas is described. The analysis is used to define the base state of the radiatively participating gas layer, just before the onset of the thermal instability, and to shed some light on the mechanisms by which thermal radiation delays the onset of instability in the gas layer.

Experiment

Experimental Apparatus

The experimental apparatus used to make the total heat transfer measurements across the carbon dioxide and air gas layers is shown in cross section in Fig. 1. The figure is drawn to scale with dimensions indicated. The apparatus, previously described by Richards,¹⁶ consists of a test cell that encloses a planar layer of gas between two rigid metal plates. The lower boundary of the test cell is an aluminum plate, and the upper boundary is a copper plate, each of width $W = 220$ mm and length $D = 450$ mm. First-surface aluminized mylar, stretched around the periphery of the hot and cold plates, makes up the sidewalls of the enclosure. The thickness of the gas layer in the test cell is set by phenolic spacers placed between the hot and cold plates.

A temperature gradient is imposed across the gas layer by electrically heating the aluminum plate at the lower boundary of the gas and water cooling the copper plate at the upper boundary of the gas. The temperatures of the hot and cold plates are measured with type-E thermocouples cemented in the plates. The total heat flux across the gas layer is determined using a guard-heated calorimeter mounted in a pocket in the center of the aluminum hot plate.

The calorimeter, 400 mm long by 100 mm wide, is constructed as a sandwich, with a brass backplate, a cork inner layer, an Inconel-foil resistance heater, and a copper faceplate. The calorimeter is mounted in a pocket machined in the aluminum hot plate, with the backplate of the calorimeter bolted tightly to the hot plate, assuring good thermal contact between the two. The copper faceplate of the calorimeter then sits flush with the front face of the aluminum hot plate, and forms the central part of the test cell's lower boundary. An eight-junction thermopile bridging the cork inner layer measures the temperature difference between the copper faceplate and the brass

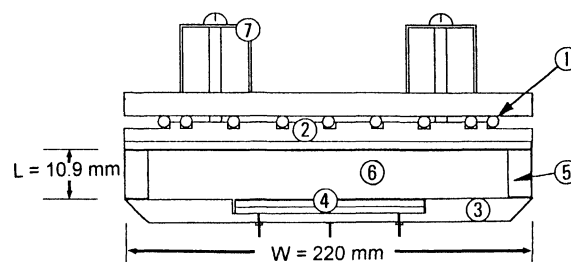


Fig. 1 Experimental apparatus in cross section showing 1, cooling water manifold; 2, cold plate; 3, hot plate; 4, calorimeter; 5, phenolic spacers; 6, gas layer; and 7, support arms.

backplate of the calorimeter. The current to the foil resistance heater is controlled in such a way as to null the voltage signal from the thermopile. When the thermopile voltage is nulled, the copper faceplate and brass backplate are at the same temperature, and all electrical power dissipated as heat in the foil resistance heater is known to be transferred out the front of the calorimeter through the copper faceplate.

The copper faceplate of the calorimeter, the face of the aluminum hot plate (lower boundary of the test cell), and the copper cold plate (upper boundary of the test cell) are kept cleaned and polished to maintain known radiative boundary conditions. For polished aluminum and copper surfaces, a value of emissivity of $\varepsilon = 0.04$ is recommended.¹⁷ Previously reported heat transfer measurements across quiescent air layers have verified the accuracy of this value of emissivity for the hot and cold plates of the present apparatus.¹⁶

The entire test cell fits into a pressure vessel so that both the gas species and their partial pressures in the test cell can be set as desired. This arrangement also allows the Rayleigh number of the gas layer to be controlled by varying the total gas pressure, while the mean temperature and the temperature gradient of the layer are held constant. Total gas pressure (gauge) in the vessel is measured with a mercury manometer, with ambient pressure determined with a mercury barometer. The entire pressure vessel can be rotated, so that the test cell can be tilted, to change the orientation of the gas layer with respect to horizontal.

In the present set of experiments, heat transfer measurements were made for gas layers of thickness $L = 10.9$ mm. This choice of gas-layer thickness was motivated by the requirement that the heat transfer behavior of the gas layer in the finite aspect ratio test cell ($D/L = 41$, $W/L = 20$) closely approximate an infinite plane layer of gas. Two aspects of this behavior were particularly important. First, it was required that the heat transfer across the gas layer approach the one-dimensional limit. Second, it was required that the onset of thermal instability not be delayed because of the presence of side walls. Previous measurements reported by Richards¹⁶ indicated that for the gas-layer thickness chosen, $L = 10.9$ mm, both the heat transfer across the gas layer and the critical Rayleigh number for the gas layer would deviate less than 1% from the case of an infinite gas layer.

Experimental Procedure

Each experimental run consists of a series of measurements of heat flux across a gas layer as the gas-layer Rayleigh number is varied by changing the total gas pressure in the test cell while the mean gas-layer temperature and temperature gradient are held constant. During a run, raw data, which consist of 1) the gas-layer temperature difference, 2) the mean gas-layer temperature, 3) the gas pressure in the test cell, and 4) the power dissipated in the calorimeter heater, are recorded every 30 s. Five minutes of measurements are then averaged together to obtain one data point.

The heat flux across the gas layer is taken to be the electrical power dissipated in the guard-heated calorimeter mounted in the face of the test cell hot plate. Two gas-layer Nusselt numbers can be defined. The first Nusselt number

$$Nu_1 = (q_{\text{cal}}/\Delta T)L/k \quad (1)$$

is the ratio of total heat transfer to the heat transfer by conduction alone across a gas layer. The second Nusselt number

$$Nu_2 = 1 + \{(q_{\text{cal}} - q_{\text{cal},0})/\Delta T\}L/k \quad (2)$$

is unity plus the ratio of the increase in heat transfer across a gas layer because of natural convection to the heat transfer by conduction alone across the quiescent gas layer. The gas-layer Rayleigh number is defined as

$$Ra = g\beta\Delta TL^3/\alpha\nu \quad (3)$$

Using the definitions of β , α , and ν , and invoking the ideal gas law, the Rayleigh number can be rewritten as

$$Ra = \frac{g\Delta TL^3 C_p P^2}{RT_m^3 \mu k} \quad (4)$$

to facilitate its evaluation. Gas properties for air and carbon dioxide are determined at the mean gas-layer temperature, T_m , from property data given by Vargaftik.¹⁸ Gas properties for mixtures of carbon dioxide and air are determined using mixture rules following Reid et al.¹⁹

The uncertainty in a measured Nusselt number can be determined as a function of the uncertainties in the measured heat flux from the calorimeter, q_{cal} , temperature difference across the gas layer, ΔT , L , and k .

Likewise, the uncertainty in Rayleigh number can be determined in terms of the uncertainties in the mean gas-layer temperature, T_m , and ΔT , L , P , k , C_p , and μ . The estimated uncertainties for these parameters are ± 0.2 K for T_m and ΔT , ± 0.01 Wm⁻² for q_{cal} , ± 0.1 mm for L , and ± 0.4 kPa for P . The gas properties, k , C_p , and μ are taken to be known to within 1% for the pure gases and to within 2% for the gas mixtures. Using these values and the method of Kline and McClintock,¹⁷ the uncertainty in measured Nusselt number is estimated to be ± 0.03 , while the uncertainty in measured Rayleigh number is estimated to range between ± 70 and ± 100 , depending on the case.

Theoretical Analysis

The quiescent, base state of the radiatively participating gas layer, before the onset of the thermal instability, is analyzed. To carry out the analysis, several simplifying assumptions are invoked. First, the gas layer is assumed to be contained between two infinite, parallel, flat plates. The plates are taken to be isothermal. The plates are also assumed to be diffuse, gray emitters, and reflectors, with the emissivities of the plates not necessarily equal. Work by Schimmel et al.⁷ indicates that application of the assumption of diffuse boundaries to a nongray gas system with specular boundaries, similar to that considered in the present study, leads to very small errors. Heat transfer in the gas layer is by conduction and radiation only, and is one dimensional and steady. All gas properties are assumed to be constant in the gas layer and are evaluated at the mean gas-layer temperature. This last assumption includes thermophysical properties such as thermal conductivity and viscosity, as well as radiative properties such as band absorptances as defined by the exponential wideband model.

Governing Equations

Under the assumed conditions, applying a heat balance to the gas layer results in

$$\frac{d}{dy} \left[k(T) \frac{dT(y)}{dy} \right] = \int_0^\infty \frac{dq_{RA}(y)}{dy} d\lambda \quad (5)$$

To solve for the temperature field in the gas layer, $T(y)$, it is first necessary to evaluate the term in the integral on the right-hand side (RHS) of Eq. (5), which represents the divergence of the total radiative flux vector. The total divergence is the integral over all wavelengths, λ , of the spectral divergence where the spectral radiative flux in the layer is²⁰

$$\begin{aligned} q_{RA}(y) = & 2J_{1\lambda} E_3(\kappa_\lambda y) - 2J_{2\lambda} E_3[\kappa_\lambda(L - y)] \\ & + 2 \int_0^y \kappa_\lambda e_{b\lambda}(t) E_2[\kappa_\lambda(y - t)] dt \\ & - 2 \int_y^L \kappa_\lambda e_{b\lambda}(t) E_2[\kappa_\lambda(t - y)] dt \end{aligned} \quad (6)$$

Here, $E_n(x)$ are the exponential integral functions, and J_1 and J_2 are the radiosities at the bounding surfaces, which are given by

$$J_{1\lambda} = \varepsilon_{1\lambda} e_{1\lambda} + (1 - \varepsilon_{1\lambda}) \times \left[2J_{2\lambda} E_3(\kappa_\lambda L) + 2 \int_0^L \kappa_\lambda e_{b\lambda}(t) E_2(\kappa_\lambda t) dt \right] \quad (7)$$

$$J_{2\lambda} = \varepsilon_{2\lambda} e_{2\lambda} + (1 - \varepsilon_{2\lambda}) \times \left[2J_{1\lambda} E_3(\kappa_\lambda L) + 2 \int_0^L \kappa_\lambda e_{b\lambda}(t) E_2[\kappa_\lambda(L - t)] dt \right] \quad (8)$$

The RHS of Eq. (5), is found by differentiating Eq. (6) with respect to the spatial coordinate, y , and then integrating over all wavelengths. The integration is accomplished by first employing the exponential kernel approximation, and then the exponential wideband model. When the result is substituted back into the heat balance, Eq. (5), we obtain

$$\begin{aligned} \frac{d^2\Theta(\bar{y})}{d\bar{y}^2} = & -\frac{3}{2} \sum_i N_i \left(\int_0^1 \tilde{e}_i(t) \frac{d\Theta(t)}{dt} \right. \\ & \times \sum_{n=0}^{\infty} (\rho_1 \rho_2)^n \left\{ \rho_1 \bar{A}'_i \left[\frac{3}{2} \tau_{0i} [2n + \bar{y} + t] \right] \right. \\ & + \rho_1 \rho_2 \bar{A}'_i \left[\frac{3}{2} \tau_{0i} [2(n+1) - \bar{y} + t] \right] \\ & - \rho_1 \rho_2 \bar{A}'_i \left[\frac{3}{2} \tau_{0i} [2(n+1) + \bar{y} - t] \right] \\ & \left. \left. - \rho_2 \bar{A}'_i \left[\frac{3}{2} \tau_{0i} [2(n+1) - \bar{y} - t] \right] \right\} dt \right. \\ & \left. - \int_0^{\bar{y}} \tilde{e}_i(t) \frac{d\Theta(t)}{dt} \bar{A}'_i \left[\frac{3}{2} \tau_{0i} (\bar{y} - t) \right] dt \right. \\ & \left. + \int_{\bar{y}}^1 \tilde{e}_i(t) \frac{d\Theta(t)}{dt} \bar{A}'_i \left[\frac{3}{2} \tau_{0i} (t - \bar{y}) \right] dt \right) \quad (9) \end{aligned}$$

Here temperature has been nondimensionalized with respect to the hot boundary temperature: $\Theta(\bar{y}) = T(\bar{y})/T_1$ and $\bar{y} = y/L$, so that $\Theta(0) = 1$ and $\Theta(1) = T_2/T_1$, and blackbody radiosity has been nondimensionalized by the radiosity at the hot boundary: $\tilde{e}_\omega(t) = e'_{b\omega}[T(t)]/e'_{b\omega}(T_1)$, where $e'_b(T) = de_b(T)/dT$. The sum on i is over all significant absorption bands, whereas the infinite sum over n accounts for interreflections between the upper and lower boundaries of the gas layer. Equation (9) reduces to the special case of boundaries with equal reflectivities, previously derived by Schimmel et al.,⁷ when ρ_1 is set equal to ρ_2 .

The total radiative flux can be obtained by employing a similar approach, again using the exponential kernel approximation and integrating over all wave numbers using the exponential wideband model:

$$\begin{aligned} q_R(\bar{y}) = & \sum_{n=0}^{\infty} (\rho_1 \rho_2)^n \{ (\varepsilon_1 e_{b1} + \rho_1 \varepsilon_2 e_{b2}) - (\varepsilon_2 e_{b2} + \rho_2 \varepsilon_1 e_{b1}) \} \\ & + \sum_i \left\{ [(\varepsilon_2 e_{b2} + \rho_2 \varepsilon_1 e_{b1}) - (\varepsilon_1 e_{b1} + \rho_1 \varepsilon_2 e_{b2})] A_{0i} \bar{A}'_i (3\tau_{0i} n) \right. \\ & + \frac{3}{2} A_{0i} \tau_{0i} \left[\rho_1 \int_0^1 (e_{b1}(t) - \varepsilon_2 e_{b2}) \bar{A}'_i \left(\frac{3}{2} \tau_{0i} (2n + t + \bar{y}) \right) dt \right. \\ & \left. \left. - \rho_2 \int_0^1 (e_{b1}(t) - \varepsilon_1 e_{b1}) \bar{A}'_i \left(\frac{3}{2} \tau_{0i} [2(n+1) - t - \bar{y}] \right) dt \right] \right\} \end{aligned}$$

$$\begin{aligned} & + \rho_1 \rho_2 \int_0^1 e_{b1}(t) \bar{A}'_i \left(\frac{3}{2} \tau_{0i} [2(n+1) - t + \bar{y}] \right) dt \\ & - \rho_1 \rho_2 \int_0^1 e_{b1}(t) \bar{A}'_i \left(\frac{3}{2} \tau_{0i} [2(n+1) + t - \bar{y}] \right) dt \Big] \Big\} \\ & + \sum_i \left\{ \int_0^{\bar{y}} \left[e_{b1}(t) \bar{A}'_i \left(\frac{3}{2} \tau_{0i} [\bar{y} - t] \right) \right. \right. \\ & - \sum_{n=0}^{\infty} (\varepsilon_1 e_{b1} + \rho_1 \varepsilon_2 e_{b2}) \bar{A}'_i \left(\frac{3}{2} \tau_{0i} [2n - t + \bar{y}] \right) \Big] dt \\ & - \int_{\bar{y}}^1 \left[e_{b1}(t) \bar{A}'_i \left(\frac{3}{2} \tau_{0i} [t - \bar{y}] \right) \right. \\ & \left. \left. - \sum_{n=0}^{\infty} (\varepsilon_2 e_{b2} + \rho_2 \varepsilon_1 e_{b1}) \bar{A}'_i \left(\frac{3}{2} \tau_{0i} [2n + t - \bar{y}] \right) \right] dt \right\} \quad (10) \end{aligned}$$

For the case of black boundaries ($\varepsilon_1 = \varepsilon_2 = 1$), Eq. (10) reduces to the result previously given by Sparrow and Cess.²⁰

Numerical Solution

The heat balance on the gas layer, Eq. (9), is solved numerically by employing a finite difference scheme that reduced the nonlinear integro-differential equation to a set of coupled algebraic equations. The full set of equations can be written in tridiagonal matrix form and evaluated using a tridiagonal matrix solver described by Press et al.²¹ The one-dimensional grid for the finite difference scheme employed 2000 equally spaced nodes. Increasing the number of nodes in the scheme beyond 2000 points caused changes in the final results on much less than 1%.

It was necessary to truncate the infinite sums in both Eqs. (9) and (10), which accounted for interreflection in the gas layer. For the numerical runs reported here, n was limited to 50 interreflections. Results for $n = 200$ interreflections were also computed and found to be indistinguishable from the runs for $n = 50$ interreflections.

The solution procedure consisted of assuming a temperature profile and then iterating on Eq. (9). In the present case, the initial temperature profile was taken to be a linear profile. Once the temperature profile was determined, Eq. (10) was used to determine the total radiative flux. The iteration was continued until two convergence criteria for the temperature profile were met. The first criterion required the current, j , and previous, $(j - 1)$, iterations of the temperature profile to be less than a threshold value:

$$\sum_{k=1}^N |\Theta_i(k) - \Theta_{i-1}(k)| \leq 10^{-4} \quad (11)$$

The second criterion of convergence of the solution depended on the standard deviation of the total heat flux across the gas layer. Because heat transfer across the gas layer is steady, the total heat flux should be constant throughout the medium. Thus, the run was considered acceptable if the standard deviation of the total heat flux at each point was less than 0.04.

Results and Discussion

Seven experimental runs were made, during which total heat transfer across gas layers were measured before, during, and immediately after the onset of thermal instability. Table 1 lists the nominal conditions for each run. Runs 1 and 2 were made with diathermanous gas layers (air). Runs 3 and 4 were made with a mixture of carbon dioxide and air, with the carbon dioxide at the relatively low partial pressure of 33 kPa. Runs 5 and 6 were made with pure carbon dioxide, with the total pressure of the gas near 95 kPa at the onset of instability. In all three cases, runs were made at two tilt angles of 0 deg (horizontal) and 30 deg. Run 7 was made with pure carbon

dioxide at an orientation of 180 deg. This orientation, with the test cell hot plate above the cold plate (heated from above), was a stable configuration, so that the gas layer was quiescent at all pressures.

Heat Transfer Before the Onset of Instability: Coupled Conduction–Radiation

Measurements of total heat transfer across a quiescent layer of carbon dioxide made during run 7 are shown in Fig. 2. In the figure, the measured Nusselt number, Nu_1 , is plotted against the total gas-layer pressure over a range from 60 to 130 kPa. The estimated uncertainty of 3% in Nusselt number is indicated with error bars on the data. The total Nusselt number predicted by the coupled conduction–radiation heat transfer analysis, employing an exponential wideband model for the nongray radiation properties of carbon dioxide, is shown with a solid line. For purposes of comparison, the total Nusselt number predicted by a coupled conduction–radiation analysis employing a gray gas model for carbon dioxide is indicated with a dashed line.

The comparison between the experimental measurements of total Nusselt number and the nongray analysis (wideband model) is seen to be within the estimated uncertainty of the measurements. Both measurements and analysis show a very small increase in total heat transfer with the increase in gas pressure. Because conduction heat transfer is independent of

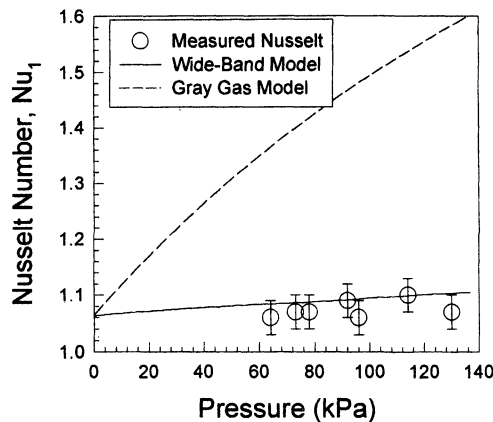


Fig. 2 Measured Nusselt number, Nu_1 , vs gas pressure for a horizontal carbon dioxide layer heated from above (180-deg tilt angle).

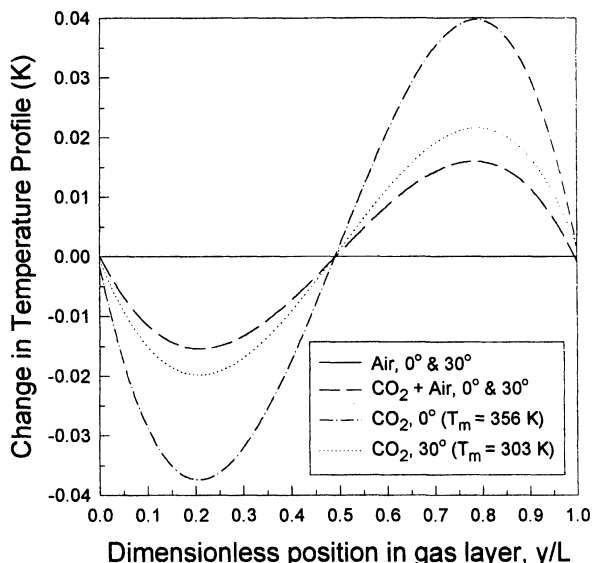


Fig. 3 Change in temperature from the linear conduction-only temperature profile vs dimensionless gas-layer position.

gas pressure over this pressure range, the figure indicates the insensitivity of the gas radiation heat transfer to gas pressure. In contrast, the gray gas analysis grossly overpredicts the contribution of gas radiation to the total heat transfer, and the effect of gas pressure on the gas radiation.

The nongray coupled conduction–radiation heat transfer analysis was subsequently used to predict the temperature profile, just before the onset of instability for runs 1–6. These temperature profiles are shown in Fig. 3. However, because in all cases, the change from the conduction-only linear temperature profile due to the contribution of gas radiation was very small, the results of the analysis are plotted as the deviation of the predicted temperature profile from a linear temperature profile. Therefore, the solid horizontal line represents the linear temperature profile for the air layer (runs 1 and 2), in which heat transfer was by conduction only. The dashed line, dotted line, and dash–dotted line represent the deviation from a linear temperature profile for the gas layers consisting of 1) a mixture of carbon dioxide and air (runs 3 and 4), 2) a layer of pure carbon dioxide at 0-deg tilt and a low mean gas-layer temperature (run 5), and 3) a layer of pure carbon dioxide at 30-deg tilt and a high mean layer temperature (run 6), respectively. In runs 3 and 4, the partial pressure of the carbon dioxide was 33 kPa, while in runs 5 and 6 the pressure of the carbon dioxide was 95 kPa.

The pressure of the radiatively participating gas is seen to have little impact on the effect of gas radiation in shifting the gas-layer temperature profile away from the linear conduction-only profile. Increasing the carbon dioxide gas pressure by a factor of 3 from 33 kPa in runs 2 and 4 to 95 kPa in run 6, while keeping the mean gas-layer temperature constant, has the effect of increasing the maximum predicted deviation from the linear profile only about 30% (from 0.016 to 0.021 K). This insensitivity of the gas radiation to the gas pressure is in agreement to the results seen in Fig. 2. In contrast, the mean gas-layer temperature has a much larger effect on the quiescent gas-layer temperature profile. Increasing the mean gas-layer temperature from 303 K in run 6 to 356 K in run 5, while holding the participating gas pressure constant, causes the maximum-predicted deviation from the linear profile to nearly double from 0.021 to 0.040 K. This increase in the effect of the gas radiation corresponds to the increase in the blackbody radiosity, which nearly doubles over the temperature range from 303 to 356 K.

Onset of Thermal Instability

Total heat transfer measurements made around the onset of thermal instability, during runs 1–6, are shown in Figs. 4–6. Figure 4 shows heat transfer measurements for air (runs 1 and 2), Fig. 5 shows measurements for the mixture carbon dioxide and air (runs 3 and 4), and Fig. 6 shows measurements for pure carbon dioxide (runs 5 and 6). In each of the figures, the first Nusselt number, Nu_1 , is plotted against Rayleigh number for the gas layer.

Before the onset of thermal instability, total heat transfer across the quiescent layer is constant as Rayleigh number increases, because heat transfer is by conduction and radiation only. After the onset of instability, heat transfer rises as the natural convective heat transfer across the gas layer increases with Rayleigh number. The critical Rayleigh number for each run is taken to be the intersection of the horizontal line fitted to the subcritical data and the upward sloping line fitted through the supercritical data. Critical Rayleigh numbers found in this way from the data in Figs. 4–6, along with estimated uncertainties, are listed in Table 1. Also given in the last column in Table 1 are the ratios of the measured critical Rayleigh numbers to the critical Rayleigh numbers predicted by linear stability theory for a diathermanous gas layer. The ratio of measured to predicted critical Rayleigh numbers gives a measure of the delay in the onset of instability caused by gas radiation.

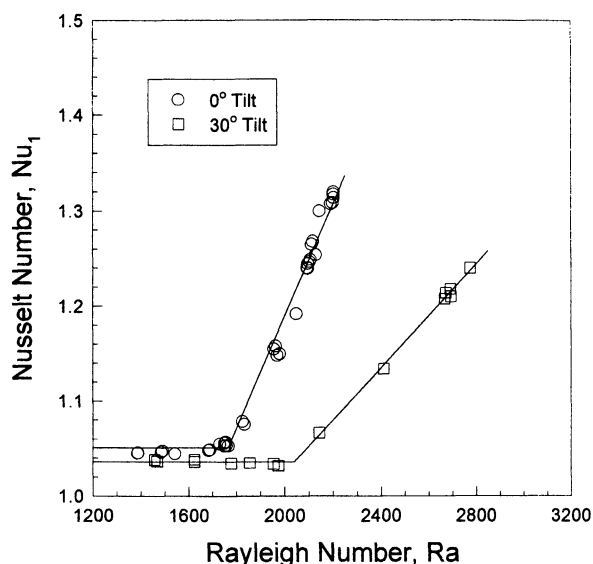


Fig. 4 Measured Nusselt number, Nu_1 , vs Rayleigh number for air layers at tilt angles of 0 and 30 deg.

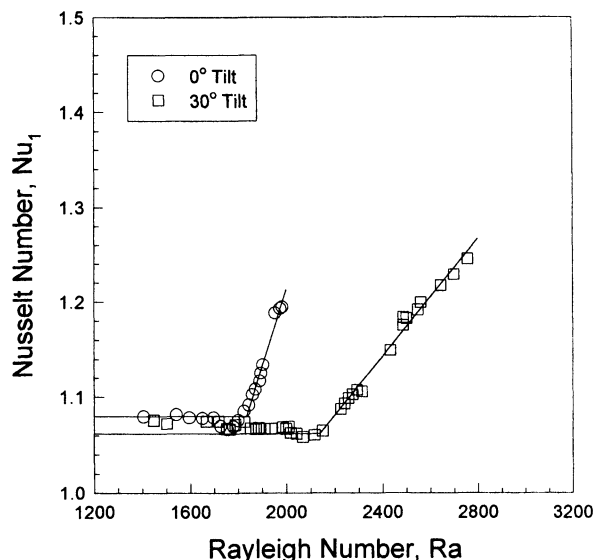


Fig. 5 Measured Nusselt number, Nu_1 , vs Rayleigh number for air and carbon dioxide gas layers at tilt angles of 0 and 30 deg.

For runs 1 and 2 with air, the measured critical Rayleigh numbers agree with the predictions of the linear theory for both the 0-deg tilt ($Ra_{cr,pred} = 1708$) and the 30-deg tilt ($Ra_{cr,pred} = 1972$) to within the experimental uncertainty. In runs 3–6, the presence of the radiatively participating carbon dioxide in the gas layer serves to delay the onset of instability by 7–8%. Increasing the pressure of the participating gas, while holding the mean gas-layer temperature constant, from runs 4 to 6 has no discernible effect on the delay in the instability. In contrast, increasing the mean temperature of the gas layer, while holding the carbon dioxide gas pressure constant from run 6 to 5, results in a significantly larger delay in the instability of 20%. Both of these results parallel the effects of gas-layer pressure and temperature on the predictions of the quiescent gas-layer temperature profiles seen in Fig. 3.

Gille and Goody³ postulated that the delay in the critical Rayleigh number for the radiatively participating gas layer resulted from two effects of the gas radiation: the distortion of the base-state temperature profile in the quiescent gas layer, and the damping of the infinitesimal temperature perturbations whose growth marks the onset of the thermal instability. The

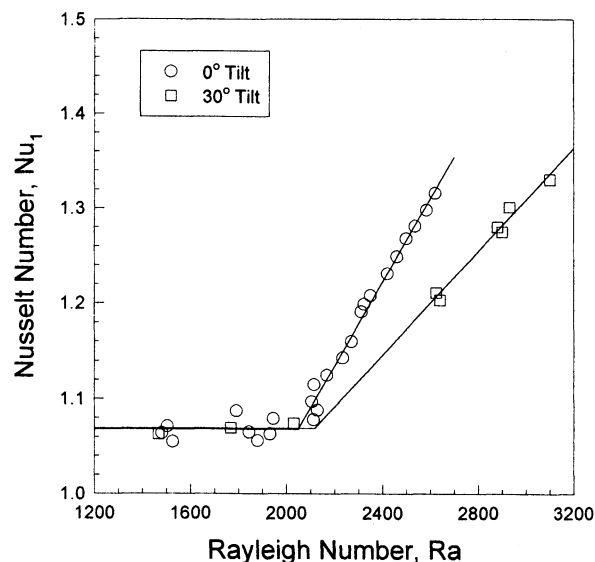


Fig. 6 Measured Nusselt number, Nu_1 , vs Rayleigh number for carbon dioxide gas layers at tilt angles of 0 and 30 deg.

first effect, the distortion of the base-state temperature profile caused by gas radiation, has been shown to be exceedingly small. The largest change from the conduction-only linear temperature profile seen in the predicted temperature profiles in Fig. 3 was the 0.04 K shift in the temperature profile of the gas layer in run 5. This shift leads to a 1% reduction in the temperature gradient at the center of the gas layer in that run, from 0.92 to 0.91 K/mm. A reduction in the temperature gradient of this magnitude would, according to Gille and Goody's approximate dimensional analysis, lead to a corresponding 1% increase in the critical Rayleigh number for run 5. Because the increase in the critical Rayleigh number measured in run 5 was 20%, it appears likely that the balance of the delay in the instability is probably a result of the second effect, the damping of small temperature perturbations by radiative heat transfer within the gas layer.

Heat Transfer After the Onset of Thermal Instability: Coupled Convection–Radiation

Total heat transfer measurements were also made across the horizontal gas layers over a wide range of Rayleigh numbers to characterize the effect of gas radiation on heat transfer after the onset of thermal instability. Figure 7 shows the measurements for the horizontal air layer, and the horizontal carbon dioxide layer, plotted as the second Nusselt number, Nu_2 , vs the gas layer Rayleigh number. Also shown in the figure are the correlations for heat transfer across a horizontal air layer recommended in Churchill²² (dotted line) and in Rohsenow et al.²³ (solid line). The figure shows the delay in the onset of the convective instability for the carbon dioxide, previously seen in Fig. 6. In addition, Fig. 7 shows that after the onset of instability, there is a 20% reduction in Nusselt number, Nu_2 , for the radiatively participating carbon dioxide compared with that found for a similar layer of diathermanous air. This 20% reduction in Nusselt number, Nu_2 , persists up to the highest Rayleigh number tested, $Ra = 10^4$.

The reason for the reduction in total heat transfer across the convecting layer of radiatively participating gas appears to be the same as that responsible for the delay in the onset of the thermal instability. The initial base-state temperature profile in the quiescent gas layer is irrelevant once the thermal instability starts up, and should have no effect on the convective heat transfer. Instead, the reduction in the convective heat transfer, like the increase in critical Rayleigh number in the participating gas layer, appears to be because of the stabilizing effect

Table 1 Experimental conditions and measured critical Rayleigh numbers

Run	Gas-layer species	Gas-layer orientation, deg	Mean gas-layer temperature, K	Gas-layer temperature difference, K	Measured critical Rayleigh number	Ratio of measured to predicted ^a critical Rayleigh numbers
1	Air	0	300	14	1760 ± 70	1.03 ± 0.04
2	Air	30	300	14	2040 ± 70	1.03 ± 0.04
3	CO ₂ + Air	0	300	14	1830 ± 100	1.07 ± 0.06
4	CO ₂ + Air	30	300	14	2140 ± 100	1.08 ± 0.05
5	CO ₂	0	356	10	2050 ± 90	1.20 ± 0.05
6	CO ₂	30	303	7	2120 ± 90	1.07 ± 0.05
7	CO ₂	180	303	7	N/A	N/A

^aCritical Rayleigh number predicted by linear stability theory for a diathermanous gas layer. For a tilt angle of 0 deg (horizontal layer), $Ra_{cr,pred} = 1708$, and for a tilt angle of 30 deg, $Ra_{cr,pred} = 1972$.

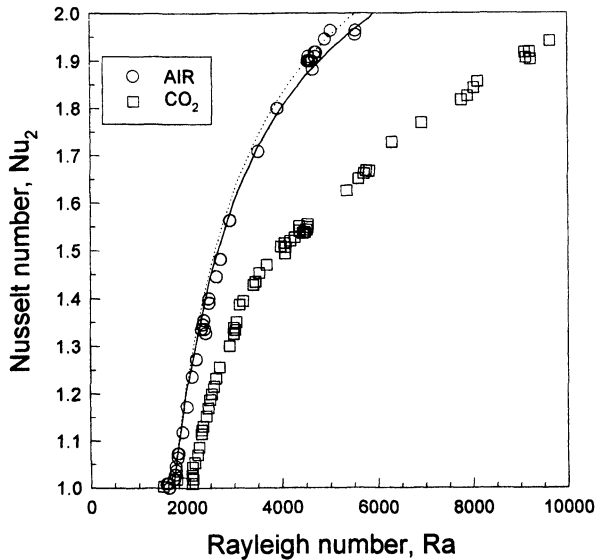


Fig. 7 Measured Nusselt number, Nu_2 , vs Rayleigh number for a horizontal air layer and a horizontal carbon dioxide layer (0-deg tilt angles).

of the gas radiation in transporting energy from hot spots to cold spots in the convecting gas.

Conclusions

Experimental measurements and analytical predictions of heat transfer across plane gas layers heated from below and cooled from above have been presented. The experimental measurements consist of total heat flux measurements across layers of both a diathermanous gas layer (air) and radiatively participating gas layers (a carbon dioxide–air mixture and pure carbon dioxide). The analytical predictions of total heat flux across and temperature profiles in the gas layers are provided by a nongray analysis of the coupled conduction–radiation heat transfer problem in a radiatively participating gas layer.

The measurements of total heat flux across the gas layers clearly show the onset of thermal instability in each of the test cases. In the radiatively participating layers, gas radiation acts to delay the onset of thermal instability. At mean gas-layer temperatures near ambient, $T_m = 300$ K, the delay in critical Rayleigh number is 7–8%. A moderate increase in mean gas-layer temperature to $T_m = 350$ K results in a much larger delay in a critical Rayleigh number of 20%. Variation in the pressure of the participating species, carbon dioxide, has little effect on the delay in critical Rayleigh number.

Analytical predictions of coupled conduction–radiation heat transfer across a quiescent gas layer based on gray gas and nongray gas models were compared with measurements of total heat transfer across a stable, quiescent layer of carbon dioxide heated from above and cooled from below. While the

gray gas model was shown to be totally inadequate, heat transfer predictions of the nongray gas model compared well with the experimental measurements. In addition, predictions of the base-case temperature profiles, just before the onset of thermal instability in each of the participating gas layers, were presented. The shift in the quiescent base-state gas-layer temperature profile, away from the linear conduction-only temperature profile, because of gas radiation, was seen to be extremely small. Increasing mean gas-layer temperature resulted in much larger changes in this shift away from the linear temperature profile than varying participating gas pressure.

Finally, total heat transfer measurements for a wide range of Rayleigh numbers were presented for layers of air and carbon dioxide. The measurements show a 20% reduction in Nusselt number, Nu_2 , across the layer of radiatively participating carbon dioxide when compared to the heat transfer across a layer of nonparticipating air. The reduction in heat transfer persists long after the onset of the thermal instability, up to the highest Rayleigh number tested, $Ra = 10^4$.

References

- Goody, R. M., "The Influence of Radiative Transfer on Cellular Convection," *Journal of Fluid Mechanics*, Vol. 1, 1956, pp. 424–435.
- Pellew, A., and Southwell, R. V., "On Maintained Convective Motion in a Fluid Heated from Below," *Proceedings of the Royal Society, Series A: Mathematical and Physical Sciences*, Vol. 176, 1940, pp. 312–343.
- Gille, J., and Goody, R. M., "Convection in a Radiating Gas," *Journal of Fluid Mechanics*, Vol. 20, Pt. 1, 1964, pp. 47–79.
- Christophorides, C., and Davis, S. H., "The Convective Instability in a Radiating Fluid Layer," *Physics of Fluids*, Vol. 13, No. 2, 1970, pp. 222–226.
- Arpaci, V. S., and Gozum, D., "Thermal Stability of Radiating Fluids: The Benard Problem," *Physics of Fluids*, Vol. 16, No. 5, 1973, pp. 581–588.
- Neitzel, G. P., Smith, M. K., and Bolander, M. J., "Thermal Instability with Radiation by the Method of Energy," *International Journal of Heat and Mass Transfer*, Vol. 37, No. 18, 1994, pp. 2909–2915.
- Schimmel, W. P., Novotny, J. L., and Olsofka, F. A., "Interferometric Study of Radiation-Conduction Interaction," *Proceedings of the 4th International Heat Transfer Conference*, Vol. 3, Elsevier, New York, 1970 (Paper R2.1).
- Novotny, J. L., and Olsofka, F. A., "The Influence of a Non-Absorbing Gas in Radiation-Conduction Interaction," *AIAA Paper 70-836*, June 1970.
- Crosbie, A. L., and Viskanta, R., "Interaction of Heat Transfer by Conduction and Radiation in a Nongray Planar Medium," *Warme und Stoffübertragung*, Vol. 4, 1971, pp. 205–212.
- Soufiani, A., Hartmann, J. M., and Taine, J., "Validity of Band-Model Calculations for CO₂ and H₂O Applied to Radiative Properties and Conductive-Radiative Transfer," *Journal of Quantitative Spectroscopy and Radiative Transfer*, Vol. 33, No. 3, 1985, pp. 243–257.
- Gupta, R. P., Wall, T. F., and Truelove, J. S., "Radiative Scatter by Fly Ash in Pulverized-Coal Fired Furnaces: Application of the Monte Carlo Method to Anisotropic Scatter," *International Journal of Heat and Mass Transfer*, Vol. 26, No. 16, 1983, pp. 1649–1660.

¹²Smith, T. F., Al-Turki, A. M., Byun, K. H., and Kim, T. K., "Radiation and Conduction Transfer for a Gas/Soot Mixture Between Diffuse Parallel Plates," *Journal of Thermophysics and Heat Transfer*, Vol. 1, No. 1, 1987, pp. 50-55.

¹³Kamiuto, K., "Combined Conduction and Nongray Radiation Heat Transfer in Carbon Dioxide," *Journal of Thermophysics and Heat Transfer*, Vol. 10, No. 4, 1996, pp. 701-704.

¹⁴Kamiuto, K., "Two-Parameter Wideband Spectral Model for the Absorption Coefficients of Molecular Gases," *Journal of Thermophysics and Heat Transfer*, Vol. 9, No. 3, 1995, pp. 569-573.

¹⁵Hutchison, J. E., "The Onset of Thermal Instability in a Radiatively Participating Medium," M.S. Thesis, Washington State Univ., Pullman, WA, 1996.

¹⁶Richards, R. F., "Thermal Stability of a Diathermanous Fluid in a Multilayer System," *International Journal of Heat and Mass Transfer*, Vol. 17, No. 14, 1994, pp. 2101-2111.

¹⁷Kline, S. J., and McClintock, F. A., "Describing Uncertainties in Single-Sample Experiments," *Mechanical Engineering*, Vol. 75, No. 1, 1953, pp. 3-8.

¹⁸Vargaftik, N. B., *Tables on the Thermophysical Properties of Liquids and Gases*, 2nd ed., Hemisphere, Washington, DC, 1975.


¹⁹Reid, R. C., Prausnitz, J. M., and Poling, B. E., *The Properties of Gases and Liquids*, McGraw-Hill, New York, 1987.

²⁰Sparrow, E. M., and Cess, R. D., *Radiation Heat Transfer*, Hemisphere, Washington, DC, 1978.

²¹Press, W. H., Teukolski, S. A., Vetterling, W. T., and Flannery, B. P., *Numerical Recipes in Fortran*, 2nd ed., Cambridge Univ. Press, New York, 1992.

²²Churchill, S. W., *Heat Exchanger Design Handbook*, VDI-Verlag GmbH, Hemisphere, Washington, DC, 1983.

²³Rohsenow, W. M., Hartnett, J. P., and Ganic, E. N., *Handbook of Heat Transfer Fundamentals*, 2nd ed., McGraw-Hill, New York, 1985.



Focusing on
scientific
and technical
information,
AIAA Dispatch
can deliver what
you need, when
you need it.

The aerospace community's premiere

DOCUMENT DELIVERY SERVICE

FEATURING MORE THAN

2 MILLION

REFERENCES.

For more information
or
to place an order:

- Call us at
800/662-1545
- or
816/363-4600
- Fax us at
816/926-8794
- Send us an e-mail
message at
dispatch@lhl.lib.mo.us
- Visit the Linda Hall
Web site at
<http://www.lhl.lib.mo.us>

AEROSPACE
ACCESS
INFORMATION SERVICES FROM AIAA

AMERICAN INSTITUTE OF
AERONAUTICS AND ASTRONAUTICS

in cooperation with the Linda Hall Library.

AIAA